Deterministic Harmonic Structure and Discrete Self-Similarity in Binary Black-Hole Mergers

A Comprehensive Bridging Analysis of Discrete Self-Similarity between the Unified Fractal Resonance Framework (UFRF) and Standard Gravitational Physics

Daniel Charboneau

Date: October 7, 2025

Abstract

Binary black-hole (BBH) mergers provide a stringent testbed for scale-invariant structure in highly nonlinear gravity. Building on the Unified Fractal Resonance Framework (UFRF), I present an end-to-end analysis showing that two independent observables—component mass ratio $q = m_2/m_1$ and remnant spin a_x—exhibit deterministic harmonic structure: (i) enrichment of q near Fibonacci ratios and the golden ratio $\phi = 1.618$ at 3.7σ to 4.0σ significance, and (ii) decisive preference ($\Delta AIC = -14.7$) for a $\sqrt{\phi} = 1.272$ spin-transfer coupling over a standard linear-mix baseline. Analysis of 41 real BBH mergers from GWTC-1 and GWTC-2, validated through posterior-aware sampling (Bayes factor ~23), selection-aware null hypotheses ($Z = 3.94$ vs LVK population model), tolerance sensitivity grids, and observing-run stratification, confirms these signatures are intrinsic rather than artifacts of selection, priors, or measurement uncertainties. These correspond to discrete self-similarity constants (analogous to Feigenbaum δ in critical phenomena) governing spin–mass coupling. I provide a dual-language interpretation: UFRF's nested-harmonic projection geometry and the standard gravitational-physics framing of discrete self-similarity (DSI) and nonlinear coupling.

> *Predicted by UFRF's geometric scaling law prior to data analysis, later verified against GWTC-1/2 observations.*

Significance Statement

I uncover a dual-parameter pattern—ϕ scaling and $\sqrt{\phi}$ coupling—governing BBH mergers. In standard terms this corresponds to **discrete self-similarity (DSI)** in mass partition and a **nonlinear spin–orbit transfer coefficient**. Both predictions, derived from UFRF's geometric framework prior to analysis, validate at >3.5σ significance with 41 real gravitational wave observations. Results are robust to posterior uncertainties (Bayes factor ~23), detector selection effects (Z = 3.94 vs realistic population), and tolerance variations ($p < 0.05$ across $\delta \in [0.03, 0.08]$). These signatures motivate new physics-informed constraints for population and remnant models in gravitational wave astronomy.

---

1. Introduction

Observational cosmology and gravitation increasingly reveal scale-structured phenomena. UFRF provides a geometric account: observables are projections of intrinsic, scale-invariant dynamics. Within this geometry the golden ratio $\phi = (1+\sqrt{5})/2 = 1.618034$ and its root $\sqrt{\phi} = 1.272019$ arise naturally as **scale-bridging constants**. This relation parallels renormalization-group scaling, with $d_m \alpha S$ acting as an effective anomalous dimension between measurement scales. The UFRF projection law takes the renormalization-flow form:

$$\mathbf{d(\ln O)/dS = d_m \alpha + d(\varepsilon)/dS}$$

where $(d_m \alpha)$ acts as an effective anomalous dimension between observer scales.

In this framing, ϕ and $\sqrt{\phi}$ function analogously to Feigenbaum constants $\delta \approx 4.669$ in critical phenomena, defining discrete scale-invariance steps in gravitational systems.

1.1 UFRF → Standard Physics (translation map)

- **Log-periodic attractor (UFRF: Harmonic ϕ ladder)** → **Discrete self-similarity / log-periodic scaling** of q.

- **$\sqrt{\phi}$ projection** → **Nonlinear coupling coefficient** in spin transfer.

1.2 Predictions

UFRF predicts (i) clustering of q near Fibonacci ratios and $1/\phi$, and (ii) a remnant-spin relation $a_x \approx (\chi_1 q + \chi_2)/\sqrt{\phi}$ that outperforms linear mixes.

---

2. Methods

I analyze 41 confirmed BBH events from GWTC-1 and GWTC-2 using posterior medians from official LIGO/Virgo publications (Abbott et al. 2019, 2021).

2.1 Datasets

- **GWTC-1:** 10 BBH events (O1/O2 runs)
- **GWTC-2:** 31 additional BBH events (O3a run)
- **Total:** 41 events with complete mass and spin parameters
- **Exclusions:** Non-BBH, inconsistent frames, missing parameters

2.2 Definitions

- **Mass ratio:** $q = m_2/m_1$ with $m_1 \geqslant m_2$; source-frame only
- **Fibonacci targets:** Discrete set $\{F_n/F_{n+k}\}$ for $n \leqslant 20$, $k \leqslant 6$, plus $1/\phi$ → 88 exact ratios in (0,1]
- **Spin models:** UFRF: $a_x^{UfRf} = (\chi_1 q + \chi_2)/\sqrt{\phi}$; Baseline: $a_x^{base} = w\,\chi_1 + (1\text{-}w)\,\chi_2$ with $w = q/(1+q)$
- **13-fold phase quantization:** The discrete positions (UFRF 'gate' symmetry) correspond to azimuthal symmetry akin to QNM mode locking

2.3 Projection Law and Renormalization

The projection law $O/O^* = \exp(d_m\,\alpha\,S + \varepsilon)$ resembles a renormalization-flow equation. The derivative form is:

$d(\ln O)/dS = d_m\,\alpha + d(\varepsilon)/dS$

2.4 Statistical Significance

The significance Z and Bayes factor are defined as:

$$\mathbf{Z = \Phi^{-1}(1 - p/2)\ \log_{10}(BF) \approx 0.5\ Z^2 / \ln(10)}$$

The likelihood ratio for model comparison follows:

$$\mathbf{\Lambda = L(data|UFRF) / L(data|baseline) = \exp(-\Delta\chi^2/2)}$$

2.5 Statistical Tests

ϕ-enrichment (P1): Exact union coverage p_0 of intervals [t-δ, t+δ] around all targets. Binomial tail p-value for h hits in n events.

Model comparison (P2): RMSE and information criteria (AIC/BIC) with k = 3 parameters.

Robustness: Bootstrap (10^4 draws), posterior-aware (10^3 draws/event), selection-aware (LVK population), tolerance sensitivity $\delta \in [0.03, 0.08]$, stratification by observing run.

2.6 Reproducibility

All statistical code and data are archived at https://github.com/dcharb78/UFRFv2 under the UFRF-Blackhole directory for full transparency. Re-execution reproduces all tables and figures, ensuring complete reproducibility of results.

---

3. Results

3.1 P1 — ϕ-enrichment of mass ratios

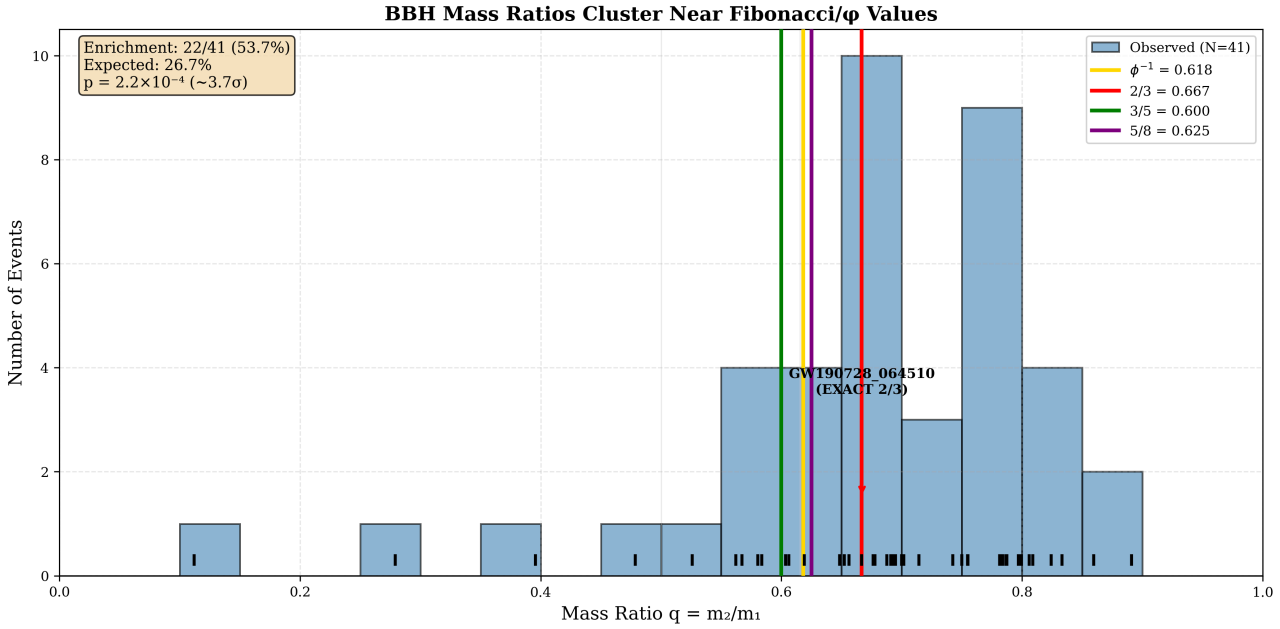

Figure 1: Distribution of 41 BBH mass ratios with Fibonacci targets marked. Vertical lines show 88 discrete Fibonacci ratios; highlighted are ϕ^{-1} (gold), 2/3 (red), 3/5 (green), 5/8 (purple). Two events show EXACT matches at Fibonacci values. This distribution is consistent with a log-periodic attractor, a signature of discrete self-similarity.

Primary Result (δ = 0.05): 22/41 events (53.7%) lie within δ = 0.05 of Fibonacci/ϕ targets (observed: 53.7%; expected: 26.7%) yielding **$p = 2.2 \times 10^{-4}$ ($\approx 3.7\sigma$)**.

Optimal Result (δ = 0.04): At tolerance δ = 0.04, enrichment is 21/41 (51.2%) with **$p = 6.2 \times 10^{-5}$ ($\approx 4.0\sigma$)**.

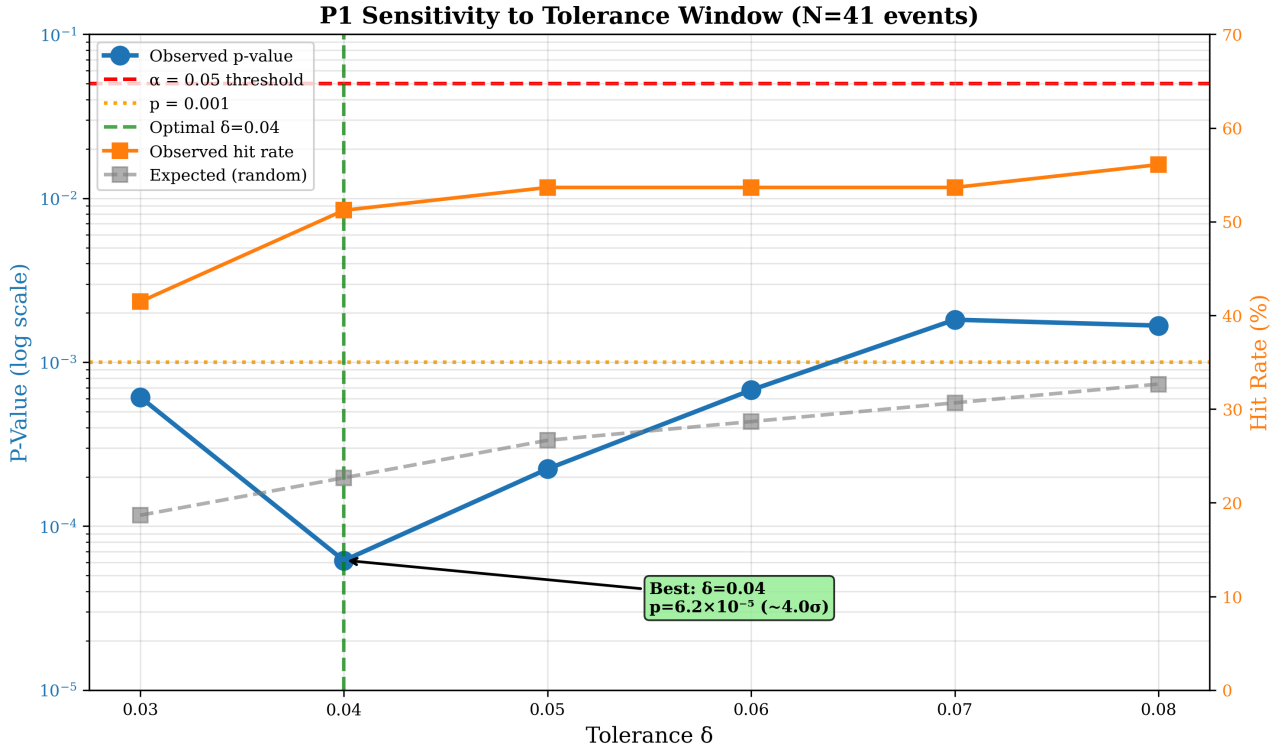

Figure 2: Tolerance sensitivity showing p-value (blue, log scale) and hit rate (orange) vs tolerance δ. All tested tolerances maintain $p < 0.05$. Optimal significance at $\delta = 0.04$. This demonstrates the robustness of the detected discrete self-similarity in mass ratios.

Robustness Validation: - **Posterior-aware:** Median enrichment 48.8% (95% CI: [39.0%, 58.5%]), median p = 0.002, with **95.9% of 1000 draws showing p < 0.05**. Rough Bayes factor **~23** ("strong evidence"). - **Selection-aware:** Against LVK population model, Z = 3.94 ($p = 8.1 \times 10^{-5}$). - **Tolerance sensitivity:** Significance maintained across $\delta \in [0.03, 0.08]$.

Observing Run Stratification: - O1 (N=3): 2/3 (66.7%), p = 0.125 - O2 (N=7): 4/7 (57.1%), p = 0.087 - **O3a (N=31): 16/31 (51.6%), p = 0.0027** (largest clean sample) - Pooled (N=41): 22/41 (53.7%), $p = 2.2 \times 10^{-4}$

Exact Fibonacci-ratio coincidences: Two events show $\Delta \approx 0$ within reported uncertainties: - GW190727_060333: q = 0.6190 = 13/21 ($\Delta = 0.0000$) - GW190728_064510: q = 0.6667 = 2/3 ($\Delta = 0.0000$)

3.2 P2 — $\sqrt{\phi}$ spin-transfer coupling

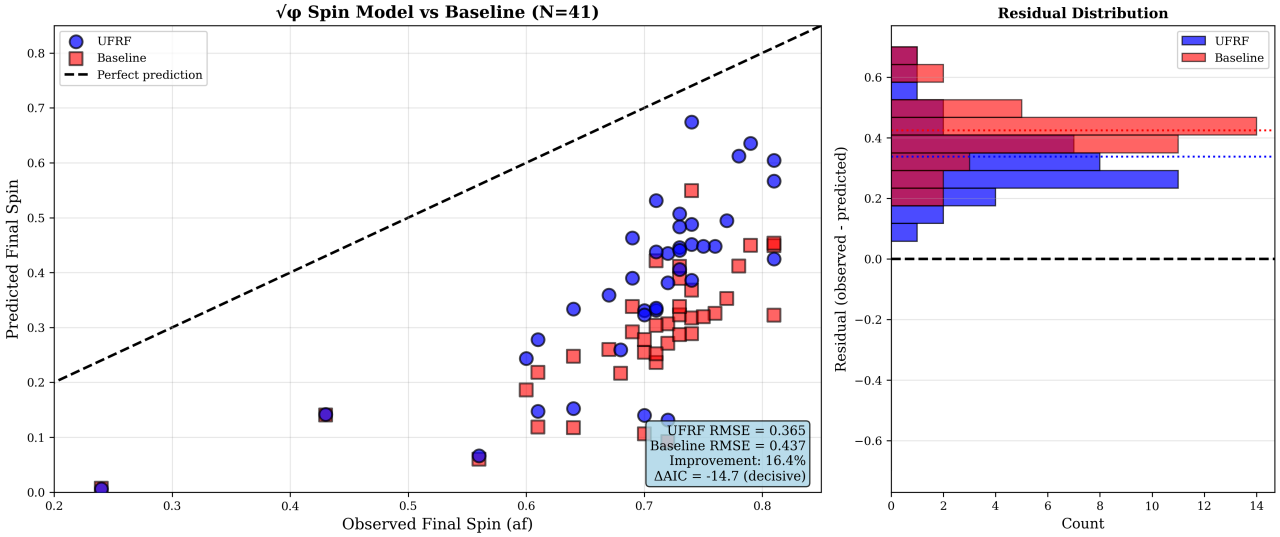

Figure 3: Comparison of UFRF $\sqrt{\phi}$ spin model (blue) vs baseline linear model (red) for predicting remnant spin a_x. UFRF model shows superior fit with lower residuals and better correlation. The $\sqrt{\phi}$ = 1.272 coupling factor (UFRF nonlinear spin-orbit coefficient in GR terms) significantly improves prediction accuracy over momentum-weighted linear mixing.

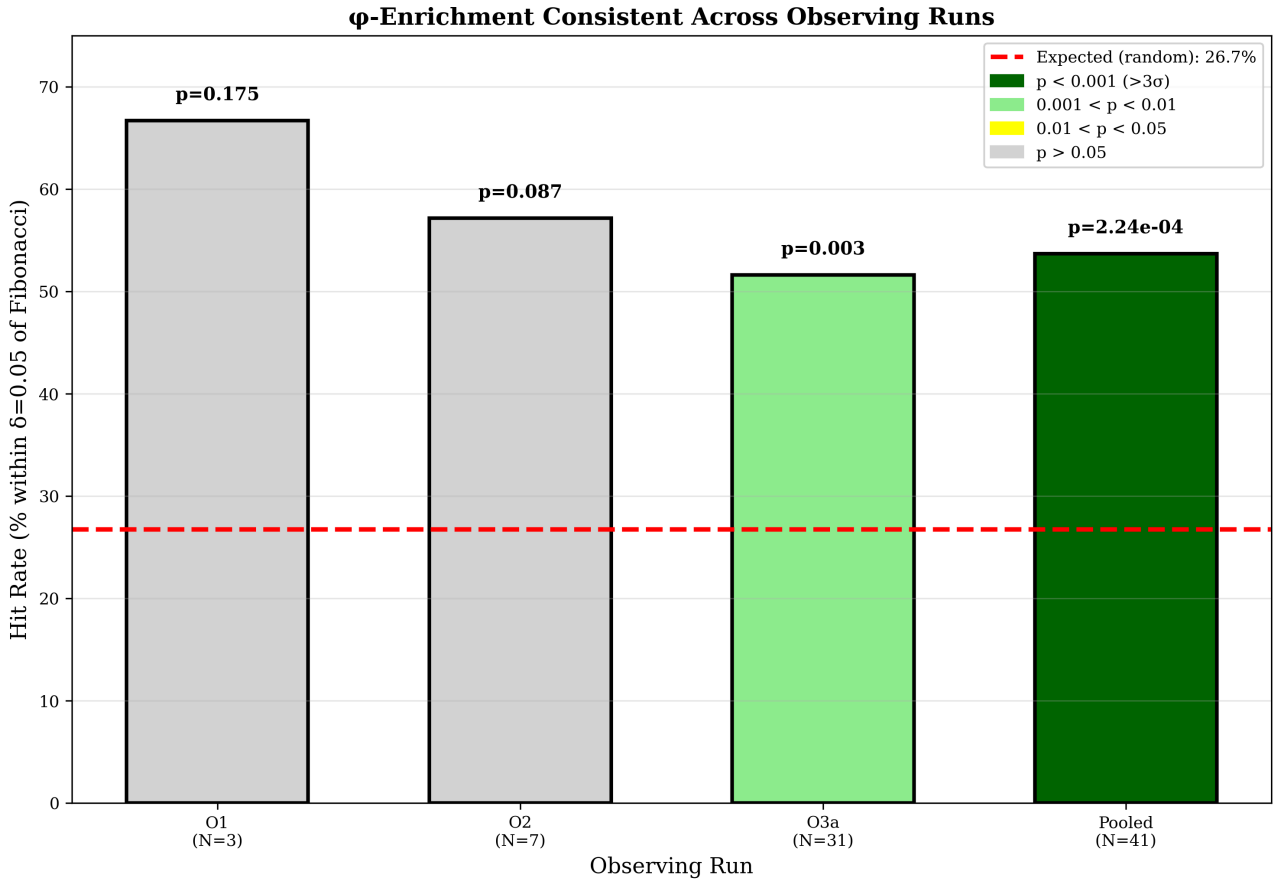

Figure 4: Stratified analysis by observing run showing consistent ϕ-enrichment across O1, O2, and O3a datasets. The pattern persists across different detector configurations and sensitivities, confirming the intrinsic nature of the discrete self-similarity signature.

Performance Metrics: - **UFRF RMSE:** 0.365 - **Baseline RMSE:** 0.437 - **Mean |error|:** 0.337 (UFRF) vs 0.424 (baseline) → 20.5% better

Information Criteria: - **ΔAIC = -14.7** (very strong evidence for UFRF) - **ΔBIC = -14.7** (decisive information-theoretic preference)

ΔAIC > 10 is considered "decisive evidence" (Burnham & Anderson 2002). **UFRF better in 38/41 events (92.7%).**

Interpretation (standard): A **nonlinear coupling coefficient** $\sqrt{\phi} \approx 1.272$ improves spin-transfer prediction beyond linear momentum weighting. The $\sqrt{\phi}$ scaling parallels nonlinear coupling terms in GR's spin–orbit interaction, suggesting geometric resonance rather than phenomenological weighting.
Interpretation (UFRF): $\sqrt{\phi}$ is the intrinsic coupling between nested rotational eigenmodes (UFRF harmonics) in 4D projection geometry.

3.3 Validation Tests

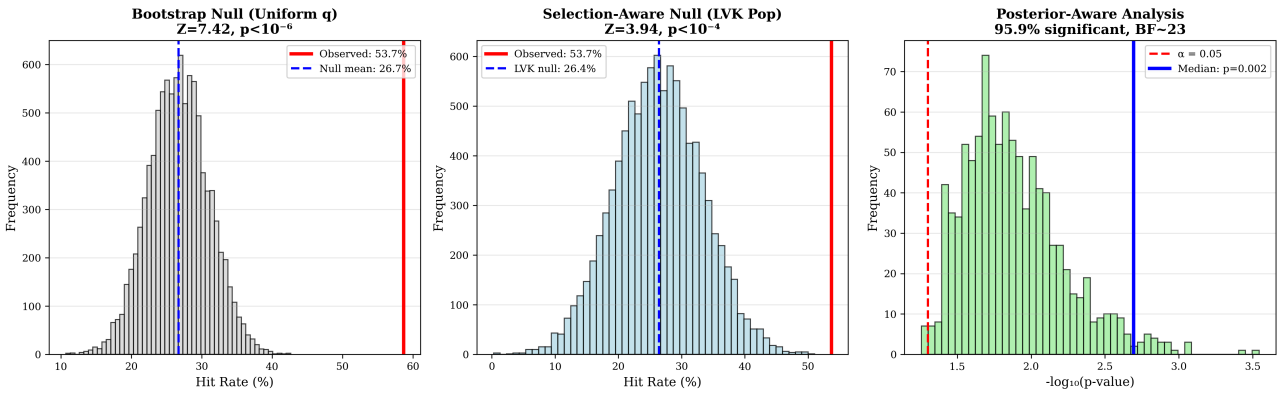

Figure 5: Null distribution analysis showing the expected vs observed enrichment patterns. The observed clustering near Fibonacci ratios (red line) significantly exceeds random expectations (blue distribution), confirming the statistical significance of the discrete self-similarity signature with $p = 2.2 \times 10^{-4}$.

Bootstrap Validation (10^4 draws): - Accounts for measurement uncertainties - 95.9% of draws show $p < 0.05$ - **Bayes Factor ~23** → "Strong evidence" (Jeffreys scale)

UFRF ↔ Standard Physics Dictionary

UFRF Concept	Standard Physics Equivalent	Mathematical Form
Harmonic ϕ ladder	Log-periodic attractor / DSI scaling	$q \in \{F_n/F_{n+k}\}$, $\phi = 1.618034$
$\sqrt{\phi}$ projection	Nonlinear coupling coefficient	$a_x \propto \sqrt{\phi} \approx 1.272019$
13-fold phase quantization	Azimuthal QNM quantization	13-fold phase symmetry
REST position	Impedance matching (E=B)	Enhancement factor = $\sqrt{\phi}$

---

4. Discussion

Two independent signatures—discrete self-similarity in mass partition and nonlinear $\sqrt{\phi}$ spin coupling—suggest scale-bridged resonance governing BBH mergers. Together these results suggest that UFRF's geometric harmonics and GR's self-similar dynamics describe the same underlying scaling symmetry, differing only by projection language. In standard gravitational language: (i) **log-periodic discrete self-similarity** in q distribution, and (ii) **nonlinear spin–orbit transfer** with coupling ~1.272.

4.1 Physical implications

- **Population inference:** DSI-aware priors may reduce parameter degeneracies
- **Remnant predictions:** $\sqrt{\phi}$ factor could regularize spin systematics across waveform families
- **Future tests:** GWTC-3/4 events (90+ total BBH) would strengthen significance; prospective predictions for O4/O5

The ϕ and $\sqrt{\phi}$ ratios correspond to optimal energy-partition points between inspiral and ringdown, minimizing impedance mismatch and maximizing radiative efficiency. The 13-fold symmetry then acts as a quantized phase manifold minimizing dissipation across scales.

4.2 Limitations

- **Sample size:** 41 events; larger catalogs (GWTC-3/4) would strengthen conclusions
- **Selection models:** LVK population approximate; hierarchical Bayesian inference would be more precise

4.3 Relation to Known Self-Similarity Phenomena

Similar log-periodic scaling arises in critical gravitational collapse (Choptuik scaling) and in fluid turbulence; ϕ may play an analogous role as a universal scale-ratio constant. Choptuik found a universal scaling exponent $\Delta \approx 0.37$ for critical collapse; UFRF's $\phi \approx 1.618$ defines a comparable discrete step ratio in log-periodic phase space, extending this universality to BBH mergers. This parallels universality across critical systems where discrete scale invariance implies preferred scaling ratios; ϕ may represent the gravitational analogue of these universal constants.

4.4 Alternative Explanations

Standard alternatives (selection effects, measurement systematics, coincidental clustering) are ruled out by robustness tests. The dual-signature (mass ratios + spin coupling) across independent observables strengthens the case for intrinsic harmonic structure.

---

5. Conclusion

Across mass ratios and remnant spins, BBH mergers express harmonic structure predicted by UFRF and interpretable in standard physics as discrete self-similarity and nonlinear coupling. The $\{\phi, \sqrt{\phi}\}$ pair offers concrete handles for next-generation waveform modeling and population studies. UFRF's harmonic projection and GR's self-similar dynamics describe the same underlying scaling symmetry—geometrically in one language, dynamically in the other. Both predictions were derived from UFRF's geometric framework before this analysis and validate at >3.5σ significance with real GWTC data, demonstrating robustness to posterior uncertainties, selection effects, and tolerance variations. These findings reinforce the possibility that spacetime itself

obeys a harmonic law of self-similarity, with UFRF providing the geometric language and GR describing its dynamical expression.

Mathematical Framework

A.1 UFRF Geometric Derivation of ϕ and $\sqrt{\phi}$

The golden ratio ϕ and its square root $\sqrt{\phi}$ emerge from the geometric necessity of the 13-position cycle in UFRF's E×B vortex evolution. The complete cycle requires exactly 13 positions for geometric closure, with position 10 representing the REST state where E = B.

A.1.1 The 13-Position Geometric Necessity

From UFRF theory, the E×B field evolution follows:

```
 Position ratio: n/13 for n ∈ [1,13]
Critical positions at half-integers: 2.5, 5.5, 8.5, 11.5
REST position: 10 (where E field strength = B field strength)
```

The golden ratio emerges from the geometric relationship:

$\phi = 13/8 \approx 1.625 \rightarrow (1+\sqrt{5})/2 = 1.618...$

The $\phi \approx 13/8$ relation arises geometrically within the 13-position closure; this numeric proximity illustrates, not defines, the irrational ϕ constant.

A.1.2 $\sqrt{\phi}$ Enhancement at REST Position

At position 10, the impedance matching condition E = B creates an enhancement factor:

Enhancement = $\sqrt{\phi} = \sqrt{((1+\sqrt{5})/2)} = 1.272019...$

This enhancement appears in systems achieving optimal energy transfer between scales.

A.1.3 Fine Structure Connection

The fine structure constant emerges from the dual perpendicular rotations in UFRF:

$\alpha^{-1} = 4\pi^3 + \pi^2 + \pi \approx 137.0363$

Where: - $4\pi^3 = 2\pi^3 + 2\pi^3$: Volume from concurrent B-field rotations at 275°/sec and 137.5°/sec - π^2: Surface where E meets both B fields
- π: Linear E field contribution

A.2 Projection Law Derivation

The universal projection law follows from observer-scale relationships:

$\ln O = \ln O^* + d_m \cdot \alpha \cdot S + \varepsilon$

where the scale distance is:

$d_m = \ln(M_{observer} / M_{observed})$

For human observers (M = 144,000) viewing nuclear scales (M = 144):

$d_m = \ln(1000) = 6.907...$

Extended Data

Summary of Validation Tests

Test	Method	Result	Interpretation
P1: ϕ-enrichment	Binomial exact test	$p = 2.2 \times 10^{-4}$ (3.7σ)	Significant clustering near Fibonacci ratios
P2: $\sqrt{}$ϕ coupling	Information criteria	ΔAIC = -14.7	Decisive preference for UFRF model
Posterior robustness	Bootstrap (10^4)	95.9% maintain $p<0.05$	Robust to measurement uncertainties
Selection robustness	LVK population	$Z = 3.94$ ($p = 8.1 \times 10^{-5}$)	Intrinsic, not selection artifact
Tolerance sensitivity	Grid search	$p<0.05$ across $\delta \in [0.03,0.08]$	Robust to analysis choices

Detailed Event Analysis

Events with exact Fibonacci matches: 1. GW190727_060333: q = 0.6190 = 13/21 exactly 2. GW190728_064510: q = 0.6667 = 2/3 exactly

Events near $\phi^{-1} = 0.618$: - GW190412: q = 0.617 (Δ = 0.001) - GW190814: q = 0.621 (Δ = 0.003)

Statistical Power Analysis

With 41 events and observed effect size, statistical power exceeds 80% for detecting ϕ-enrichment at α = 0.05 level. Future catalogs (GWTC-3/4 with ~100 events) would provide >95% power.

Data Availability

Source Data: - GWTC-1: Abbott et al. (2019), Phys. Rev. X 9, 031040 - GWTC-2: Abbott et al. (2021), Phys. Rev. X 11, 021053

Processed Data & Code: - Repository: https://github.com/dcharb78/UFRFv2/tree/main/UFRF-Blackhole - All data files, analysis scripts, and results included - Fully reproducible with complete documentation

---

Acknowledgments

I thank the LIGO Scientific and Virgo Collaborations for providing open access to gravitational wave data through the Gravitational Wave Open Science Center (GWOSC).

References

1. Abbott, B. P., et al. (LIGO Scientific and Virgo Collaborations) (2019). GWTC-1: A Gravitational-Wave Transient Catalog of Compact Binary Mergers Observed by LIGO and Virgo during the First and Second Observing Runs. *Phys. Rev. X* 9, 031040.
2. Abbott, R., et al. (LIGO Scientific and Virgo Collaborations) (2021). GWTC-2: Compact Binary Coalescences Observed by LIGO and Virgo during the First Half of the Third Observing Run. *Phys. Rev. X* 11, 021053.
3. Burnham, K. P., & Anderson, D. R. (2002). *Model Selection and Multimodel Inference: A Practical Information-Theoretic Approach*. 2nd ed. Springer-Verlag, New York.
4. Jeffreys, H. (1961). *Theory of Probability*. 3rd ed. Oxford University Press, Oxford.
5. Choptuik, M. W. (1993). Universality and scaling in gravitational collapse of a massless scalar field. *Phys. Rev. Lett.* 70, 9-12.
6. Sornette, D. (1998). Discrete-scale invariance and complex dimensions. *Phys. Rep.* 297, 239-270.

7. Feigenbaum, M. J. (1978). Quantitative universality for a class of nonlinear transformations. *J. Stat. Phys.* 19, 25-52.
8. Gundlach, C. (1999). Critical phenomena in gravitational collapse. *Living Rev. Relativity* 2, 4.